# Shedding Light on the Nature of Photoinduced States Formed in a Hydrogen-Generating Supramolecular RuPt Photocatalyst by Ultrafast Spectroscopy

Huijser, Annemarie; Pan, Qing; van Duinen, David; Laursen, Mads G.; El Nahhas, Arnal; Chabera, Pavel; Freitag, Leon; Gonzalez, Leticia; Kong, Qingyu; Zhang, Xiaoyi

*Published in:*
The Journal of Physical Chemistry. A: Molecules, Spectroscopy, Kinetics, Environment, & General Theory

*DOI:*
10.1021/acs.jpca.8b00916



*Publication date:*
2018

THE JOURNAL OF PHYSICAL CHEMISTRY A

Article

Cite This: J. Phys. Chem. A 2018, 122, 6396−6406

pubs.acs.org/JPCA

# Shedding Light on the Nature of Photoinduced States Formed in a Hydrogen-Generating Supramolecular RuPt Photocatalyst by Ultrafast Spectroscopy

Annemarie Huijser,[†,◇] Qing Pan,[†,◆] David van Duinen,[†,¶] Mads G. Laursen,[‡] Amal El Nahhas,[§] Pavel Chabera,[§] Leon Freitag,[∥,+] Leticia González,[∥] Qingyu Kong,[⊥,×] Xiaoyi Zhang,[⊥] Kristoffer Haldrup,[‡] Wesley R. Browne,[#] Grigory Smolentsev,[∇,○] and Jens Uhlig*[,§,◇]

[†]Optical Sciences and PhotoCatalytic Synthesis Groups, MESA+ Institute, University of Twente, P.O. Box 217, 7500 AE Enschede, The Netherlands

[‡]Department of Physics, Technical University of Denmark, 2800 Kongens Lyngby, Denmark

[§]Department of Chemical Physics, Lund University, Getingevägen 60, Lund 22100, Sweden

[∥]Institute of Theoretical Chemistry, Faculty of Chemistry, University of Vienna, Währinger Str. 17, 1090 Vienna, Austria

[⊥]X-ray Sciences Division, Argonne National Laboratory, Argonne, Illinois 60439, United States

[#]Molecular Inorganic Chemistry Group, Stratingh Institute for Chemistry, University of Groningen, 9747 AG Groningen, The Netherlands

[∇]Paul Scherrer Institute, Villigen 5232, Switzerland

[○]Smart Materials International Research Center, Southern Federal University of Russia, Rostov-on-Don 344090, Russian Federation

Supporting Information

**ABSTRACT:** Photoinduced electronic and structural changes of a hydrogen-generating supramolecular RuPt photocatalyst are studied by a combination of time-resolved photoluminescence, optical transient absorption, and X-ray absorption spectroscopy. This work uses the element specificity of X-ray techniques to focus on the interplay between the photophysical and -chemical processes and the associated time scales at the catalytic Pt moiety. We observe very fast (<30 ps) photoreduction of the Pt catalytic site, followed by an ∼600 ps step into a strongly oxidized Pt center. The latter process is likely induced by oxidative addition of reactive iodine species. The oxidized Pt species is long-lived and fully recovers to the original ground state complex on a >10 $\mu$s time scale. However, the photosensitizing Ru moiety is fully restored on a much shorter ∼300 ns time scale. This reaction scheme implies that we may withdraw two electrons from a catalyst that is activated by a single photon.

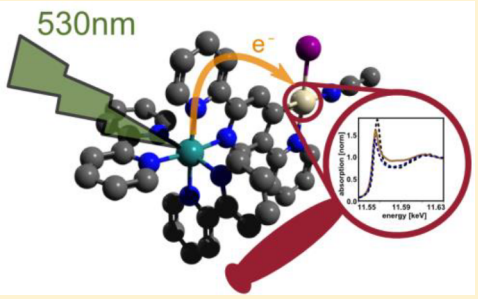




## INTRODUCTION

The impact of increasing atmospheric concentrations of $CO_2$ on life is driving the urgent development of carbon-neutral energy conversion approaches. Solar devices are generally considered to be among the most promising options for environmentally friendly renewable energy. The amount of solar energy reaching the earth in 1 h exceeds the annual global energy use,[1] illustrating the potential of converting sunlight into electricity or fuel. A key challenge faced in the use of photovoltaic cells lies in the storage of energy. This constraint has stimulated the development of photocatalytic systems that can convert sunlight into fuel directly, with light-driven generation of $H_2$ from water at the forefront of these efforts.

Among various approaches, $H_2$-generating photocatalysts that mimic photosynthesis have been studied intensively in recent years.[2−5] In these photocatalysts, an organometallic photosensitizer is bound chemically to a catalytic moiety via a bridging ligand (intramolecular approach; see Figure 1). This assembly offers key advantages over an intermolecular approach in which the photosensitizer and catalytic moiety units are mixed in solution, which relies on diffusion-limited electron transfer to the catalytic moiety to enable proton reduction.[6−8] An additional component essential in both approaches is the sacrificial agent used to regenerate the photosensitizer after light-induced electron transfer to the catalytic moiety.

Since the first reports on $H_2$-evolving Ru/M (M = Pd, Pt) organometallic supramolecular photocatalysts, independently published by Sakai[9] and Rau[10] in 2006, efforts have been made to develop efficient photocatalysts. To increase their efficiency,

Received: January 26, 2018
Revised: June 27, 2018
Published: July 27, 2018




DOI: 10.1021/acs.jpca.8b00916
J. Phys. Chem. A 2018, 122, 6396−6406

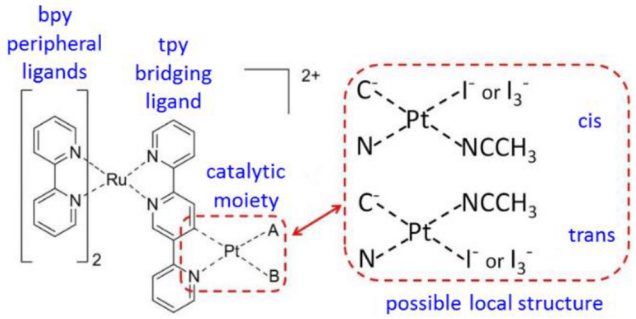


**Figure 1.** (left) Chemical structure of RuPt in anhydrous acetonitrile.[25] (right) Possible local structures of the Pt catalytic moiety in solution.

control of each of the elementary steps of the photocatalytic hydrogen generation process is essential. Mechanistic insights such as those developed here are also relevant for the development of economically attractive Cu- and Fe-based alternatives.[11−17] Many of the successful designs originate from Ru-based photocatalysts.

Time-resolved X-ray absorption spectroscopy (XAS) is a powerful method to achieve mechanistic insight into processes occurring at optically dark catalytic metal moieties. In the case of photocatalysts in particular, it is important to understand photoinduced changes in the oxidation state and coordination geometry of the reaction center. Because of the atomic selectivity of the X-ray probe, this technique can monitor the dynamics at a selected metal center and can thus be applied to probe the essential photoinduced electron transfer step to the catalytic site and the associated atomic rearrangements in real time.[17−21] Experiments at synchrotron facilities typically have a time resolution of tens of picoseconds and are well-suited to identify the fast and slow dynamics in complex systems. In addition to visualizing early-time excited-state processes, XAS experiments with microsecond time resolution were demonstrated to be capable of tracking reaction intermediates in, e.g., catalytic hydrogen evolution.[22−24] These experiments were performed on a mixture of a photosensitizer, a sacrificial agent, and a Co catalyst (i.e., the intermolecular approach) and allowed the detection of the $Co^{I}$ intermediate species formed by reduction. Importantly, the local structure of the Co catalyst was found to play a critical role in the transiently formed species and the catalytic activity. These studies illustrate the potential of time-resolved X-ray spectroscopy to develop mechanistic understanding of photocatalytic hydrogen generation.

We recently developed a series of new Ru-metal photocatalysts, of which the RuPt derivative (see Figure 1) showed a $H_2$ turnover number of 80 after 6 h of irradiation at 470 nm.[25] An important observation made is that the structure of the catalytic moiety plays a critical role in the early-time photodynamics,[26] which is generally accepted to have a major impact on the photocatalytic performance.[27,28] Femtosecond optical transient absorption measurements showed important differences between RuPt and its RuPd analogue.[26] The spectrotemporal behavior of RuPt is highly complex, indicating an ∼1 ps quenching process of the triplet metal-to-ligand charge transfer ($^3$MLCT) states localized on the individual ligands, populated after light absorption and intersystem crossing, by a lower-lying $T_3$ state. The behavior of RuPt strongly depends on the excitation wavelength, and the contribution of the $T_3$ state is particularly prevalent for excitation at relatively low photon energies. This $T_3$ state is unlikely to be localized on the ligands, as it shows very weak absorption in the blue−ultraviolet region typically associated with ligand-based transitions. The absence of such an ∼1 ps quenching process for the monomeric Ru precursor suggests that the $T_3$ state is associated with the Pt catalytic moiety. A second ultrafast process with a decay time of ∼100 ps was exclusively observed for RuPt and may thus also be related to the Pt catalytic moiety.[26]

The minor reductions in $^3$MLCT lifetime and photoluminescence quantum yield observed for RuPt and its RuPd analogue relative to their monomeric Ru precursor could suggest photoinduced electron transfer from the bridging ligand to the catalytic moiety on a long ∼100 ns time scale.[25,29] An alternative explanation is that the photoluminescence intensities and lifetimes may reflect relative populations of excited states localized at the individual ligands (with the state at the bridge potentially delocalized over the catalytic moiety[29]) rather than the dynamics of intramolecular electron transfer from the photosensitizer to the Pt moiety. Thus, the photoexcited electron density in the complex may become delocalized over the bridging ligand and the catalyst much faster than these photoluminescence data suggest. To discriminate between these two scenarios, synchrotron-based transient X-ray absorption experiments with picosecond time resolution have been pursued to identify photoinduced changes in oxidation state and the geometry of the Pt catalytic moiety. The interpretation of the time-resolved X-ray absorption data is supported by time-resolved photoluminescence and transient optical absorption data. An important feature of femtosecond transient absorption spectroscopy is that experiments can be performed at a low (kHz) repetition rate with a relatively long integration time. The low repetition rate is important to avoid a new photoexcitation step before the prior event decaying on a (sub)microsecond time scale has finalized. Fluorescence upconversion could be an alternative, provided that instead of at a high repetition rate[30] the experiments can be performed at a low repetition rate.

In the ground state, Pt is most likely in its 2+ oxidation state, as $Pt^{I}$ species are unstable, and the complex adopts the well-known square-planar coordination for which $Pt^{II}$ $d^8$ complexes are known.[31,32] As shown in Figure 1, Pt is coordinated to one C atom, one N atom, and two I atoms.[25,33] Upon dissolution in acetonitrile, one solvent molecule likely becomes coordinated to the Pt atom, substituting one $I^-$ anion.[25,33] The fourth coordination site remains occupied by an $I^-$ anion, as indicated by NMR and elemental analysis.[25] The $I^-$ anion and the solvent molecule may adopt either a cis or a trans configuration (see Figure 1). A number of photochemical reactions involving the bound and the now-free $I^-$ ions are feasible, such as the formation of $I_3^-$ at the $I^-$ coordination site or the reaction of Pt with $I_2$ or $I_2^-$ in an oxidative addition process to form a hexacoordinated Pt complex.[34−36]

The aim of this study of RuPt is thus to shed light on the nature of the optically dark $T_3$ state and understand the photochemical processes at the Pt catalytic moiety.

## EXPERIMENTAL SECTION

### Synthesis and Steady-State Optical Characterization.

The synthesis of RuPt with this bridging structure can lead to the formation of a dinuclear form with one Ru photosensitizing moiety and one Pt reaction center or to a pentanuclear form



DOI: 10.1021/acs.jpca.8b00916
J. Phys. Chem. A 2018, 122, 6396−6406

with two photosensitizer units and three connected Pt atoms, as described in detail in ref 25. The current experiments were performed on the dinuclear structure shown in Figure 1. The complexes were dissolved in acetonitrile (Sigma-Aldrich, anhydrous, purity >99.9%) and placed in 1 cm path length cuvettes for steady-state optical measurements. UV−vis absorption spectra were recorded using a Shimadzu UV-1800 spectrophotometer. Steady-state photoluminescence spectra were obtained using a Horiba Jobin Yvon FluoroMax-4 spectrofluorometer with excitation at 450 nm. Both absorption and photoluminescence spectra were recorded at room temperature.

**Time-Resolved Optical Experiments.** Transient absorption (TA) experiments were pursued in both the femtosecond−picosecond time window and the nanosecond−microsecond time window. The polarizations of the pump and probe beams were set at 54.7° to avoid anisotropy effects. The femtosecond TA setup[29] and experimental conditions[26] were described in detail earlier.

The nanosecond TA experiments were performed with a frequency-doubled, electronically delayed and triggered Nd:$YVO_4$ laser providing 3 mJ/cm$^2$, 1 ns, 532 nm pulses as the pump and a supercontinuum probe generated by focusing 800 nm, 65 fs laser pulses into a $CaF_2$ crystal. The $CaF_2$ crystal was mounted on a continuously moving stage to avoid thermal damage. The supercontinuum probe signal was dispersed by a grating and measured with a pair of diode arrays. The sample was dissolved to 0.02 mM in anhydrous acetonitrile (Sigma-Aldrich, purity >99.9%), degassed with dry Ar for 15 min, and sealed in an airtight 1 mm cuvette.

Photoluminescence decays were obtained by exciting the RuPt sample (0.02 mM in anhydrous acetonitrile, Sigma-Aldrich, purity >99.9%, degassed with dry $N_2$ for 30 min) with the frequency-doubled output of a Nd:YAG laser (532 nm). The photoluminescence signal was dispersed by a spectrograph and detected using an amplified CCD camera. The signal acquisition by the camera was gated electronically. The photoluminescence decay was obtained by integrating the recorded emission signal in a spectral window from 550 to 820 nm at various gate delays. The full width at half-maximum of the instrumental response function (Gaussian) was determined to be 4.7 ± 0.2 ns. The data were corrected by subtraction of the background dark counts.

**Steady-State X-ray Absorption Experiments.** Steady-state X-ray absorption spectra of the Pt L3 edge in the X-ray absorption near-edge structure (XANES) and extended X-ray absorption fine structure (EXAFS) regimes were obtained at beamline 11-1D-D of the Advanced Photon Source (Argonne, IL, USA) during the same measurement campaign as the transient X-ray spectra discussed below. The RuPt photocatalyst was dissolved in 75−100 mL batches to a concentration of 0.5−1 mM in anhydrous acetonitrile (Sigma-Aldrich, purity >99.9%), degassed with dry $N_2$ for 30 min, and kept in a constant $N_2$ environment during the measurement. The solution was flown in a round jet with a diameter of approximately 1 mm and a flow speed of 1−2 m/s. The total X-ray-induced fluorescence was measured by two X-ray diodes equipped with Soller slits and a Z-1 Zn foil of 6 absorption lengths. Details of the setup were reported earlier.[37] The energy was calibrated simultaneously by measuring the X-ray absorption spectra of a metallic Pt foil using the X-ray photons after the sample jet.

Because of the collection mode described in the next section, the steady-state near-edge spectra were collected continuously during the whole experimental campaign, allowing intervention once the first accumulative sample damage was observed, typically after 16−18 h of data collection. Steady-state and pump−probe XANES spectra were collected on fully refreshed parts of the jet. During data analysis, the spectra were filtered, and no data in which any (integrated) sample damage was significant were used. Damaged samples showed a distinct differential feature very different from the pump−probe signals shown in next section. The mode of data collection ensured that the steady-state XANES was collected with significantly higher statistics (approximately 4000×) than the single-bunch synchronous pump−probe experiment for the same time interval. The whole sample volume was illuminated for less than 4 min. This procedure also ensured the observation of accumulative chemical reaction(s) altering the XANES spectra, if any occurred.

**Time-Resolved X-ray Absorption Experiments.** Time-resolved X-ray absorption measurements were pursued at beamline 11-1D-D of the Advanced Photon Source. Details of the experimental setup were described in the previous section and in earlier publications.[37] The experiments were conducted in 24-bunch mode with a bunch separation of 153 ns and a typical X-ray bunch width (fwhm) of 79 ps. The sample was excited with a 527 nm laser pulse (5 ps duration, 1.6 kHz repetition rate) focused to a 500 $\mu$m diameter spot size with an intensity of ∼190 mJ/cm$^2$ per pulse. The excited spot on the flowing liquid jet was probed with the synchronized X-ray bunch at the chosen time delay after laser excitation, and the consecutive bunches were spaced in 153 ns time intervals. Bunch-to-bunch normalization allowed the use of the same X-ray bunch during multiple orbits in the storage ring and thus the study of dynamics beyond 3.6 $\mu$s with the same photoexcitation pulse. After approximately 320 $\mu$s, the laser irradiation area flew completely out of the probed region (as observed by following a linearly decaying signal and verified by estimations based on flow speed and laser focus diameter), and a number of bunches were used to collect steady-state XANES before the arrival of the next laser pump pulse, which thus excited a fully refreshed sample spot. The X-ray probe spot was approximately 50 $\mu$m (vertical) by 500 $\mu$m (horizontal), which was significantly smaller than the pump spot, and it is thus reasonable to assume a homogeneously excited sample. From the steady-state optical absorption, geometry, and pump photon flux, 79% of the molecules in the probed spot were estimated to be photoexcited, which is necessary because of a competing loss channel at the peripheral ligands.[26]

**Data Analysis.** The open-source program Glotaran[38] was used for the analysis of the femtosecond−picosecond TA data. The nanosecond optical TA data were analyzed using methods provided by the python computational package SciPy[39] and a newly developed python-based analysis suite. The data from multiple scans were averaged, and sections that showed scattered light from the pump beam were masked. The data were then binned into equal 1 nm wavelength bins and modeled by consecutive exponential decays using a 1 ns instrument response function and a global analysis scheme presented previously.[40−42] In short, a model was formed that predicts the temporal development of different species using the lifetime parameter as input. For each new set of lifetime parameters, the spectral components were assigned to each species by a least-mean-square optimization to the data. A


DOI: 10.1021/acs.jpca.8b00916
J. Phys. Chem. A 2018, 122, 6396−6406

Nelder−Mead minimization algorithm from the SciPy computational package was used to minimize $\chi^2$ by optimizing the lifetime parameter for the given model, the instrument response function, and potential time offsets. The decoupled optimization of the lifetime parameter and spectral components makes this type of analysis robust against noise in the measured transient spectra.

Steady-state EXAFS spectra were analyzed using the Athena and Artemis packages.[43] The scattering paths were calculated using FEFF 6. The analysis followed the approach recommended in the literature.[44,45] The absolute energy scale of each scan was calibrated with a simultaneously collected reference foil measurement. The parameters of the model were optimized both in $k$ and $R$ space with $k$, $k^2$, and $k^3$ weights, leading to fits of very similar quality. Different model molecules were generated with a procedural code, and their parameters were in turn refined in Artemis. In addition to this parameter refinement, a number of other structural models were tested by calculating the full multiple scattering with FEFF 8.6[46] and generating/optimizing these structures with a procedural code, followed again by an EXAFS refinement. This second procedure was necessary to test a wider range of possible structural alternatives than the simple refinement method permitted.

The XANES scans were energy-calibrated using the reference foil, scaled to an edge step of 1, and summarized for a number of different bunches of the probing X-ray light. These averaged data were compared for different periods of one sample batch and between different sample batches to exclude data from radiation-damaged molecules. Once radiation damage was observed, data from that batch were excluded from the analysis. The transient XANES for delay times of <2, 150, and 300 ns was formed by averaging the signals of single bunches following laser excitation. The transient data for longer delay times used the average of multiple consecutive X-ray bunches (spaced by 153 ns).

For modeling of the XANES at the L3 edge, a new python routine was created that combines parametric movement (translation and rotation) of single atoms or whole structural groups with control parameters describing, e.g., the electronic configuration and other calculation parameters into input files for FEFF 9.[46] This routine enables the efficient and restrained optimization of all simulation parameters or, limiting the number of recalculations, the optimization on a surface span by a few precalculations, similar to the approach in FitIt.[47] By this method, a wide variety of structures and parameters were created, allowing the XANES to be calculated and compared with the experimental spectra. The linear regression was done using the SciPy Statsmodels package.[48]

## RESULTS AND DISCUSSION

**Absorption and Fluorescence Properties.** Figure 2a shows the steady-state absorption and photoluminescence spectra of RuPt. The photoluminescence spectrum was measured for photoexcitation at 450 nm. The sharp absorption band at ∼289 nm is likely due to ligand-centered (LC) $\pi-\pi^*$ transitions of the peripheral bipyridine (bpy) ligands and the shoulder at ∼320 nm to LC $\pi-\pi^*$ transitions of the bridging 2,2′:5′,2″-terpyridine (tpy) ligand. The broad absorption band centered at 457 nm likely originates from Ru-based singlet metal-to-ligand charge transfer ($^1$MLCT) transitions to the bpy and tpy ligands.[25,26] In addition, Pt-based MLCT transitions

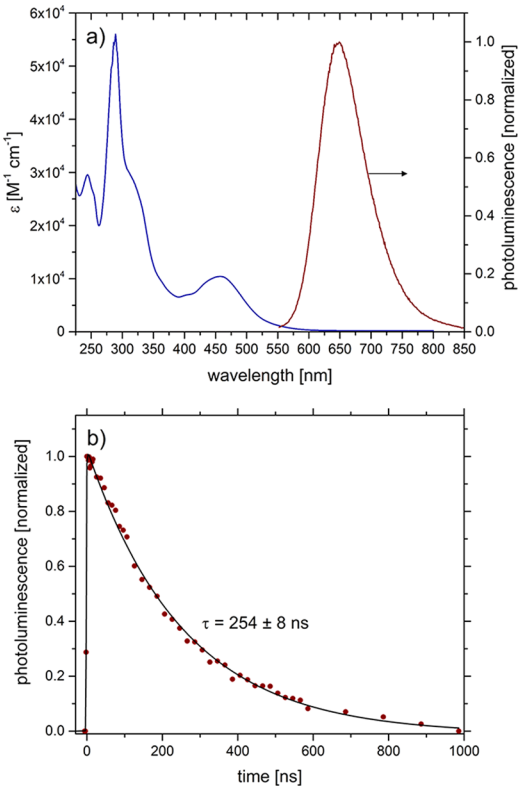


**Figure 2.** (a) Optical extinction coefficient (blue) and photoluminescence spectrum (red) of RuPt in anhydrous acetonitrile and (b) photoluminescence decay integrated from 550 to 820 nm obtained with excitation at 532 nm (red points), including a fit to a monoexponential decay function and the resulting lifetime.

observed earlier between 300 and 450 nm possibly contribute to the absorption spectrum.[49]

As intersystem crossing likely occurs very rapidly in these type of complexes (<100 fs),[50−52] the photoluminescence centered at ∼649 nm is indicative of radiative relaxation from a manifold of lowest $^3$MLCT states to the ground state.[28,29] The photoluminescence decay shown in Figure 2b was measured for photoexcitation at 532 nm. The signal was integrated over nearly the entire emission band from 550 to 820 nm because the low molar absorptivity at 532 nm results in weak emission. The photoluminescence decay is well-described by a monoexponential decay function with a lifetime of 254 ± 8 ns.

**Transient Optical Absorption.** To support the interpretation of the time-resolved X-ray absorption data discussed below, transient absorption experiments were pursued at various pump wavelengths and time windows. Figure 3a shows the femtosecond TA spectra of RuPt with excitation at 527 nm, with a strong excited-state absorption (ESA) band at >530 nm indicating population of the $T_3$ state.[26] The negative signal from 450 to 520 nm is due to ground-state bleaching (GSB). The weak ESA in the 350−450 nm window suggests a minor population of $^3$MLCT states.[26] Figure 3b shows the kinetic traces at 480 and 650 nm. The signal at 480 nm becomes less negative on an ∼1 ps time scale, indicating a potential $^3$MLCT → $T_3$ quenching process, which is more evident for excitation at higher photon energies. Photoexcitation at 516 or 480 nm (favoring the population of $^3$MLCT states) also gave a third kinetic component, indicating that ∼5 ps $^3$MLCT$_{bpy}$ → $^3$MLCT$_{tpy}$ internal conversion competes with vibrational cooling at the bpy ligands. The lack of evidence for this


DOI: 10.1021/acs.jpca.8b00916
J. Phys. Chem. A 2018, 122, 6396−6406

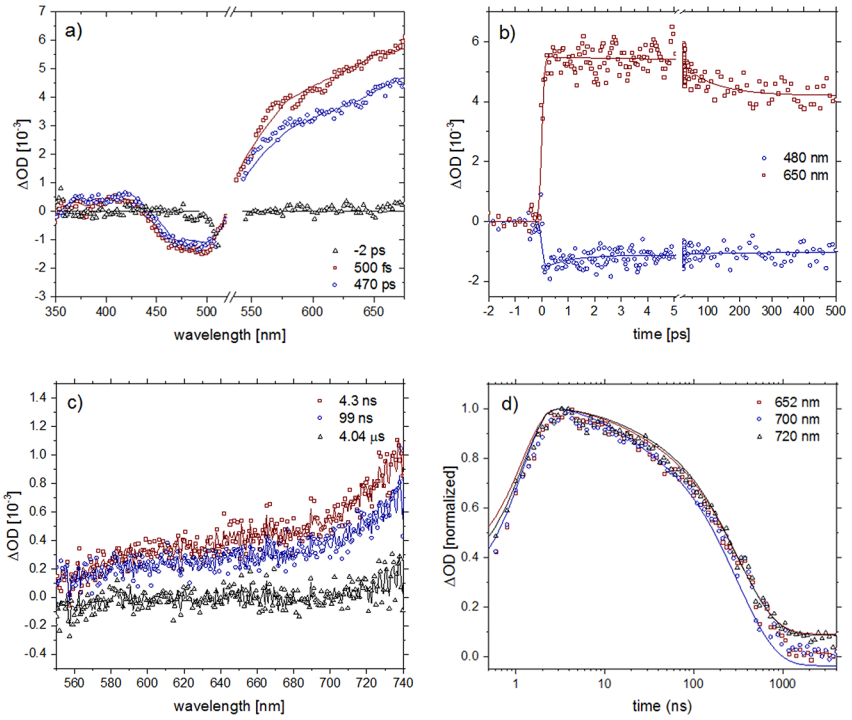


**Figure 3.** (a) Femtosecond transient absorption spectra of RuPt in anhydrous acetonitrile at 527 nm excitation and (b) kinetic traces at selected wavelengths, with fits based on a sequential model with lifetimes of 980 ± 184 fs and 99 ± 12 ps included as lines. (c) Nanosecond transient absorption spectra at 532 nm excitation and (d) kinetic traces at key wavelengths with fits based on a sequential model with lifetimes of 21 ± 5 ns and 340 ± 50 ns included as lines. The signal rise corresponds to the 1 ns excitation pulse width.

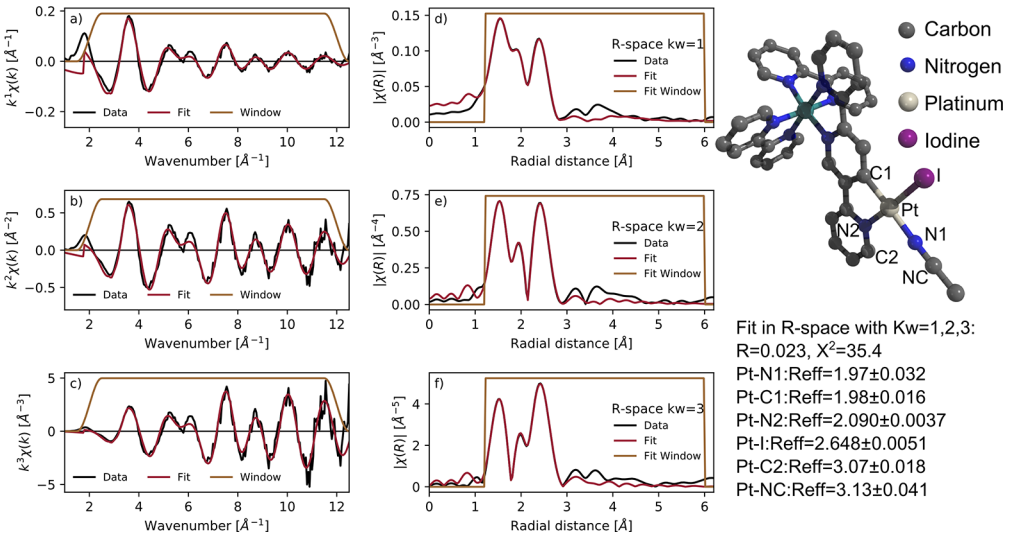


**Figure 4.** Analysis of the extended X-ray absorption fine structure spectrum. Panels (a–c) present the data and fits in *k* space for different *k* weights, and panels (d–f) show the data and windows in *R* space for different *k* weights. The fit was performed in *R* space with *k* weight (kw) = 1, 2, or 3, respectively, and paths up to 3.2 Å. Main analysis results and the corresponding structure are shown in the right panel, with distances given in Å.

process upon photoexcitation at 527 nm with the simultaneous strong ESA for the $T_3$ state indicates a nonequilibrated population of excited states with favored population of the $T_3$ state due to a lower photoexcitation energy.[26] The broad ESA at >550 nm partially decays on an ∼100 ps time scale, as illustrated by the kinetic trace at 650 nm. The nature of the $T_3$ state is unknown, although the absence of the ∼1 ps and ∼100 ps components for the Ru monomeric precursor and the RuPd analogue[26] seems to suggest an important role of the Pt catalytic moiety. As discussed in the Introduction, it is unclear when the photoelectron reaches the Pt moiety and what is the nature of the electron transfer process.

Transient optical absorption experiments were also performed in the nanosecond–microsecond time window with photoexcitation at 532 nm (Figure 3c,d). Analogous to the early-time spectra shown in Figure 3a, strong ESA at >550 nm is observed. Its spectrotemporal behavior is well-described by two time scales of 21 ± 5 and 340 ± 50 ns. The latter value is relatively close to the photoluminescence lifetime (Figure 2b), and the difference in values may be due to different experimental conditions, in particular the photoexcitation


DOI: 10.1021/acs.jpca.8b00916
J. Phys. Chem. A 2018, 122, 6396–6406

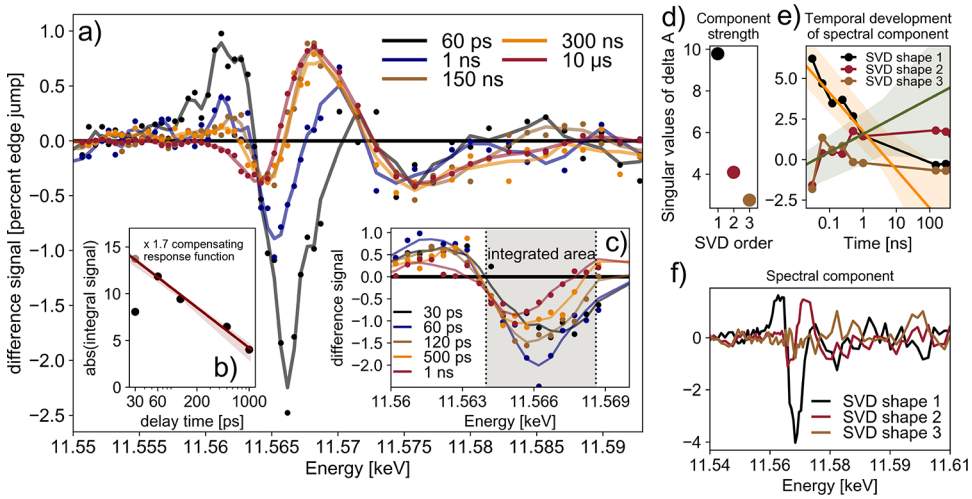


**Figure 5.** (a) Transient X-ray absorption spectra of RuPt in anhydrous acetonitrile at various time delays after 527 nm photoexcitation (dots; the lines are 3 point locally smoothed to guide the eye). (c) Zoom-in around the Pt L3 absorption edge at early time delays. (b) Signal intensity integrated over the gray area in c). The linear regression (without the 30 ps point) suggests a lifetime of 930 ± 100 ps. The time point at 30 ps is also shown, corrected for the partial overlap of the X-ray pulse and the pump pulse. (d–f) Singular value decomposition (SVD) analysis of the signal matrix: (d) total intensity of the selected SVD component; (e) temporal evolution of the first three spectral components shown in (f). The linear regression (without the 30 ps time point) suggests lifetimes of 880 ± 117 ps for SVD component 1 and 630 ± 270 ps for SVD component 2 (see the text).

intensity, concentration, and degassing conditions. The normalized kinetic traces in Figure 3d show that the decay is independent of the ESA wavelength in the probed range. The origin of the 21 ± 5 and 340 ± 50 ns decay times will be discussed below.

**Steady-State X-ray Absorption.** Figure 4 shows the analysis of the steady-state EXAFS data. The measured EXAFS was modeled by a number of different structures, including among others those of the original RuPt photocatalyst and the complex in which one or both $I^-$ anions were replaced by acetonitrile or $I_3^-$ (see section 1 in the Supporting Information (SI) for a complete list). For each structure the parameters were optimized to yield the best $\chi^2$, and the resulting structural parameters were analyzed for feasibility (results with, e.g., negative Debye–Waller factors were rejected). In the structural configuration associated with the optimum $\chi^2$, one $I^-$ anion is replaced by acetonitrile in the cis configuration (see Figure 1). The right panel of Figure 4 presents this optimized structure and its structural parameters, confirming the earlier-calculated parameters except for a slightly extended Pt–N1 bond length (1.968 ± 0.03 Å vs 2.1 Å).[25] This structure was used as the basis for all further calculations. The edge position $E_0$ corresponding to the oxidation state was optimized as part of the fitting process.

**Transient X-ray Absorption.** Figure 5a shows transient X-ray absorption spectra of RuPt at various time delays after 527 nm photoexcitation. The earliest difference absorption spectrum at 30 ps (Figure 5c) indicates that the Pt catalyst is already reduced on this time scale. The linear regression analysis (i.e., $\log_e$(intensity) versus time), presented in Figure 5b, shows that the signal intensity decreases on a 930 ± 100 ps time scale. The change in shape of the integrated signal suggests that this decay is due to more than a single component. Thus, singular value decomposition (SVD) analysis was pursued to elucidate the involvement of different spectral components. Figure 5d–f shows the results of this analysis, in which the data matrix **W**, which represents spectra corresponding to different delays, was factorized as **W** = **USV***. The first two spectral components in **U** have significant features and are shown in Figure 5f, scaled with the singular values from **S** whose values are drawn in Figure 5d.

These two spectral components have the same shape as the measured spectra at 60 ps and 10 $\mu$s (see Figure 5a), and their time evolution is thus relevant and can be analyzed. The small *S* value, spectral shape, and unphysical time evolution of the third spectral vector suggests that it has to be considered as primarily noise-related. The temporal evolution of the first two vectors was again modeled by linear regression (without the 30 ps time point, using only the time points up to 1 ns), which suggested a lifetimes of 880 ± 117 ps for SVD component 1 and 630 ± 270 ps for SVD component 2. The lifetime for the first component and the value determined from the integral in Figure 5b (930 ± 100 ps) match within the error margins. It is apparent that synchronous with the decay of the first spectral component, the growth of the second spectral component halts and is stable within this time window. There are minor differences between the spectra measured at 150 and 300 ns as well as between the spectra measured at 300 ns and 10 $\mu$s (see Figure 5a). The first spectral component has no intensity left at these measurement times.

The XANES spectra were modeled using the software package FEFF 9.6[46] with the self-consistent field potentials and multiple scattering algorithm (the full parameter set is given in SI section 2). In Figure 6a the measured ground-state XANES (brown) is shown versus the modeled ground-state XANES (black, abbreviated as GS). The ground-state model GS reproduces the measured spectrum very well, including the positions of the features at 11.575 and 11.585 keV, but slightly underestimates the total intensity in this region. This behavior has also been found in other publications.[53,54] Following the methodology established in the literature, the observed and calculated white-line intensities for this complex lie between the values typically assigned to $Pt^{II}$ and $Pt^{IV}$ complexes (also see Figure S7), and we observe a reduced Fermi parameter in the FEFF modeling, both indicating partial oxidation of the Pt catalytic center.[55,56]



DOI: 10.1021/acs.jpca.8b00916
J. Phys. Chem. A 2018, 122, 6396–6406

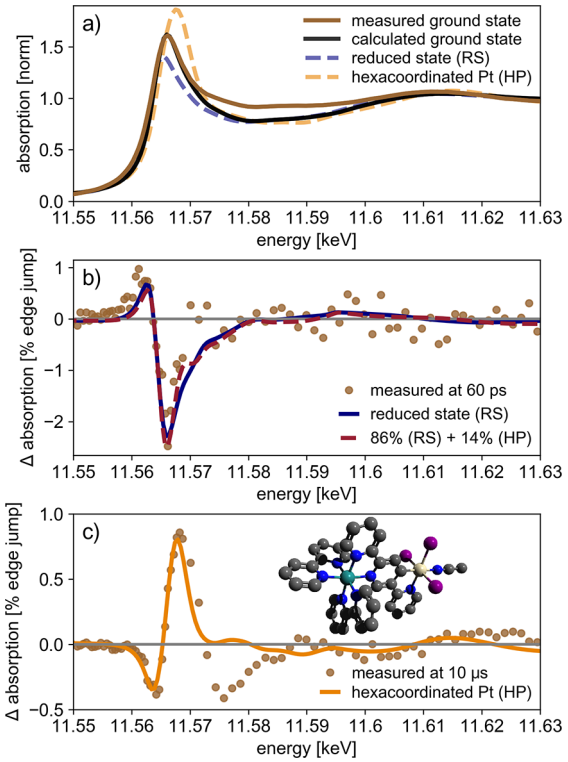


**Figure 6.** Modeling of XANES data. (a) Measured ground state spectrum (brown) compared to the calculated ground-state spectrum (black) and the spectra of two putative excited states, RS and HP. (b) Difference XANES measured at a delay of 60 ps modeled with a reduced platinum site (RS) and a linear combination of RS and HP. (c) Difference spectrum at 10 $\mu$s (brown), modeled with an oxidative addition of two iodine ions (HP). The inset shows the modeled complex.

To model the reduced state (RS), we have taken into account the higher occupancy of the d level (shift of the Fermi level by 1.0 eV), accompanied by a small chemical shift of the spectrum (0.3 eV), while keeping the same local structure of the complex. The model describes the difference spectra measured at 60 ps well (see Figure 6b). SVD analysis indicates that the transient at 60 ps is a mixture, with ca. 86% RS and 14% of the species dominant at 10 $\mu$s. This mixed model describes the shape at 11.568 keV better than the pure RS model. The white-line intensity of this species is comparable to those of $Pt^{II}$ complexes discussed in the literature (see SI section 7) and shows the clear sign of a reduction compared with the GS.[55,56] The narrow shape of the difference feature suggests that the primary process we can observe in this time window is reduction due to the electron transfer and not an oxidation process as would be expected for excitation of a Pt-based MLCT transition (see the Discussion).[49,61]

The long-lived species observed at a delay of 10 $\mu$s is characterized by a higher intensity of the white line (positive transient signal at 11.568 keV) and a shift of the absorption edge to higher energies (negative signal at the rising edge of the spectrum around 11.564 keV; Figure 5a). These are the typical signatures of Pt oxidation, suggesting a long-lived intermediate. The white-line intensity is comparable to those of $Pt^{IV}$ complexes in the literature (see SI section 7).[55,56] It is noteworthy that the observed difference spectrum is broadened further to higher binding energies than can be explained by our proposed model, which indicates the involvement of more than a single oxidation reaction.

To understand the formation of such an intermediate, it is important to point out that during the initial solvation each RuPt complex releases one $I^-$ ion, as can be understood by the difference between the crystal structure and the solvated structure discussed above. Thus, a large number of $I^-$ ions are available in solution, and two processes may occur. The first one is the formation of $I_3^-$, followed by the substitution of $I^-$ by $I_3^-$. We explored the formation of $I_3^-$ by time-resolved Raman spectroscopy at 355 nm in an effort to detect the characteristic $I_3^-$-enhanced Raman scattering, but this was not observed.

A second process suggested in the literature, combining a strong oxidation with an enhancement of the white line, is oxidative addition.[34−36,57−59] Here $I_2$ from the solution oxidizes the complex to form a hexacoordinated $Pt^{IV}$ species. We do have a significant amount of $I^-$ ions present, and it is thus likely that $I_2$ is formed, making this process possible. The strong oxidation, observed experimentally as the white-line enhancement and the failure to observe the characteristic $I_3^-$ Raman signatures, suggests that the latter is the most likely process. We thus modeled the observed oxidative process at 10 $\mu$s with the hexacoordinated Pt species shown in Figure 6c (abbreviated as HP), which shows reasonable agreement with the experiment. Alternative models with different combinations of all components available in solution occupying different bonding sites at various distances and angles (see SI section 1) gave worse agreement with the experimental data.

## DISCUSSION

Population of the $^1$MLCT, $^3$MLCT$_{bpy}$, $^3$MLCT$_{tpy}$, and $T_3$ states depends on the photoexcitation wavelength and is nonequilibrated. More excess energy leads to larger population of the $^3$MLCT$_{bpy}$ and $^3$MLCT$_{tpy}$ states and more ~5 ps $^3$MLCT$_{bpy}$ → $^3$MLCT$_{tpy}$ internal conversion competing with vibrational cooling at the bpy ligands.[26] This nonequilibrated population of excited states may be responsible for the minor effect of the excitation wavelength on the photoluminescence quantum yield (see SI section 3). The excitation wavelengths used in this work (527 and 532 nm) favor population of the $T_3$ state after photoexcitation of mostly Ru-based $^1$MLCT transitions (see SI sections 5 and 6) to the bpy and tpy ligands and ultrafast intersystem crossing.[50−52] The femtosecond transient optical absorption data indicate that this $T_3$ state is also populated via an ~1 ps $^3$MLCT → $T_3$ quenching process (Figure 3a,b). The earliest transient X-ray absorption spectrum at 30 ps (Figure 5c) already shows the reduction of the Pt site. Hence, ultrafast population of the $T_3$ state may correspond to reduction of the Pt site.

The subsequent time scale observed by transient optical absorption is ~100 ps. It should be noted that a comparable 86 ± 40 ps decay component, assigned to GSB recovery, was observed earlier for a related RuPt complex.[60] However, the cause of the ~100 ps component here is likely different, as the GSB signal (Figure 3b, difference signal at 480 nm) does not change at this time scale. The absence of a strong ~100 ps component in the X-ray data indicates that the associated process is not directly correlated to the Pt moiety. Instead, it may be related to the Ru photosensitizer.

From the time evolution of the XAS difference signal (ΔXAS), we observe first the prompt appearance of a species with the signature of reduced Pt, which decays on an 880 ±



DOI: 10.1021/acs.jpca.8b00916
J. Phys. Chem. A 2018, 122, 6396−6406

107 ps time scale (Figures 5b,e). The ΔXAS evolves in both shape and magnitude into the spectrum measured at 10 μs, indicating that a strongly oxidized species is formed on a 630 ± 270 ps time scale and has a lifetime of >10 μs. The formation of the second species does not progress after decay of the reduced species, showing that reduction of Pt is essential for this reaction. The two time scales and intensities are different, suggesting two separate decay paths from the reduced Pt.

The transient X-ray absorption results suggest two possible alternative scenarios:

1. Reduction of Pt and oxidation of Pt are completely independent processes, occurring at different coexisting RuPt photocatalysts. The first process is induced by electron transfer from the Ru photosensitizer to the Pt catalytic moiety, while oxidation could be the result of a Pt-based MLCT excitation.[49,61]
2. The initial Pt reduction step is essential to trigger the oxidation process. Hence, Pt oxidation occurs only for RuPt photocatalysts with reduced Pt centers formed in the earlier reaction step.

The observation of Pt-based MLCT transitions for Pt(II) complexes[49,61] supports scenario 1. The Pt(III) species formed after photoexcitation in this case will have a weakly axial binding character, forming bonds with the solvent, $I^-$, $I_2^-$, or even $I_3^-$. However, the Pt-based MLCT transitions reported in the literature are in the range of 300−450 nm, suggesting that for the 527 nm excitation used in the transient X-ray experiments, scenario 1 is unlikely. This hypothesis is supported by time-dependent density functional theory (TD-DFT) simulations, which indicate a dominant contribution from Ru-based MLCT transitions for excitation at 527 nm (see SI section 6). A minor contribution of Pt-based optical transitions leading to ultrafast oxidation of a small fraction of the Pt moieties is possible, however. Further evidence for scenario 2 is provided by comparison of the optical transient absorption spectra of RuPt with those of its monomeric Ru precursor (SI section 5). For both complexes, a negative band around 400−450 nm developing within the instrumental response time (100−150 fs) and slightly red-shifted relative to the UV−vis absorption spectrum is observed. This signal is most likely mainly due to GSB and likely also has a contribution from ESA. The absence of a significant effect of the Pt moiety on the GSB at early time scales after photoexcitation indicates that for RuPt Ru-based optical transitions are dominant for 527 or 532 nm excitation, as Pt-based excitations should have resulted in a clear change in GSB. Moreover, comparison of the theoretical transient XAS data for models with weak axial coordination of Pt by the solvent, single $I^-$, $I_2^-$, or even $I_3^-$ with the experimental spectra shows worse agreement with the data.

On the basis of these arguments, we suggest that the strong oxidation process we observe is oxidative addition of $I_2$ to the initially reduced Pt center, forming a hexacoordinated $Pt^{IV}$ complex.[34−36] As a random solution mixture of 0.5−1.0 mM RuPt and reactive iodine species gives a diffusion time of several nanoseconds according to the Stokes−Einstein equation, the reactive iodine species is likely present in the RuPt solvation shell. The reduced amplitude of the difference signal (despite the strong oxidation) and the lower decay rate of the initiating species suggest additional rate-limiting processes, maybe related to $I_2$. However, the large error bars of the time scales make this line of argumentation a mere suggestion that needs to be verified by additional experiments, such as X-ray studies using the iodine edge. The general time scale of <1 ns for the oxidation reaction is very short, which could suggest a prior arrangement of the reacting species.

The 21 ± 5 and 340 ± 50 ns components observed by transient absorption (Figure 3d) and the 254 ± 8 ns photoluminescence decay (Figure 2b) are nearly absent in the X-ray data, which show only minor changes between 150 and 300 ns and between 300 ns and 10 μs. The latter difference is already present at 450 ns (data not shown). The absence of a significant change in the X-ray spectra suggests that these processes are associated with the Ru moiety rather than the Pt catalyst. The complete excited-state absorption decay (Figure 3d) indicates that the photo-oxidized Ru moiety is regenerated on this time scale. We cannot distinguish between the pathways leading to ground-state recovery of the Ru moiety and thus have tentatively labeled the species differently. Figure 7 shows a Jablonski diagram of the proposed photoinduced processes.

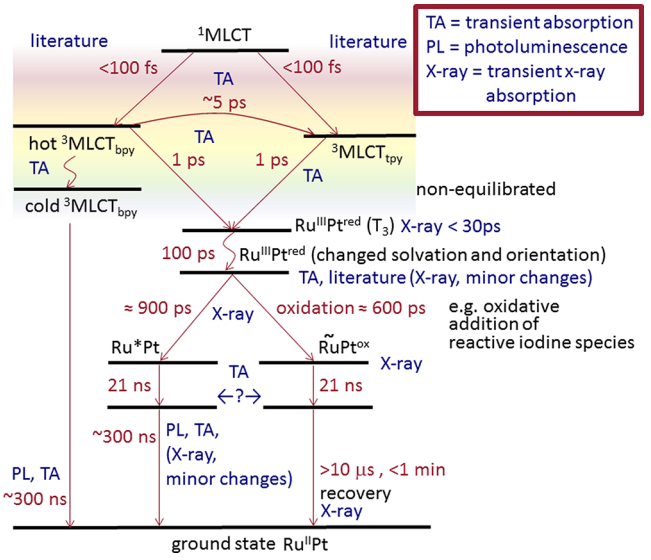


**Figure 7.** Jablonski diagram of processes occurring after photoexcitation of RuPt, with the technique supporting each individual conclusion indicated.

The likely involvement of reactive iodine species (i.e., $I^-$, $I_3^-$, and/or $I_2$) in the strong oxidation process following the photoinduced reduction of the Pt center may have important consequences for the mechanism of $H_2$ generation. The state-of-the-art design principle of supramolecular photocatalysts is based on the use of more photons (two for $H_2$ generation[62]) and requires accumulative charge separation.[63] We activate this catalyst with a single photon but possibly withdraw two electrons from the Pt moiety. Such an approach could thus potentially bypass the need for the highly challenging charge accumulation and should be investigated in more detail under catalytic conditions. This mechanism might also explain the generally higher photocatalytic activity of iodine-based photocatalysts relative to, e.g., chloride alternatives[64,65] and presents a novel paradigm for hydrogen generation by supramolecular photocatalysts.



DOI: 10.1021/acs.jpca.8b00916
J. Phys. Chem. A 2018, 122, 6396−6406

## CONCLUSION

Transient optical and X-ray absorption spectroscopy studies on light-induced electronic and structural changes of a hydrogen-generating supramolecular RuPt photocatalyst show that reduction of the Pt catalyst occurs on an ultrashort time scale (<30 ps). The population of excited states is non-equilibrated on the picosecond time scale, and vibrational relaxation competes with internal conversion toward the bridging ligand and the catalyst. Thus, not every absorbed photon leads to reduction of the Pt catalyst. The reduced intermediate species decays on a subnanosecond time scale via two processes; a part of the complexes are strongly oxidized while a second part are returning to the ground state. The strong oxidation process may be driven by oxidative addition of reactive iodine species. The oxidized intermediate is long-lived (>10 $\mu$s) and ultimately recovers into the original ground state. This reaction scheme implies that we may withdraw two electrons from a catalyst that is activated by a single photon, bypassing the need for accumulative charge separation for $H_2$ generation.

## ASSOCIATED CONTENT

### Supporting Information

The Supporting Information is available free of charge on the ACS Publications website at DOI: 10.1021/acs.jpca.8b00916.

Models tested for difference XANES and EXAFS structure characterization, FEFF parameters used for calculation of models, photoluminescence at various excitation wavelengths, differential absorption spectra under reduction conditions, transient absorption spectra at various excitation wavelengths, TD-DFT calculations of optical transitions, and comparison of white-line intensities of modeled and measured XANES (PDF)

## AUTHOR INFORMATION


### Corresponding Author

*E-mail: jens.uhlig@chemphys.lu.se.

### ORCID

Pavel Chabera: 0000-0002-0531-5138
Leon Freitag: 0000-0002-8302-1354
Leticia González: 0000-0001-5112-794X
Qingyu Kong: 0000-0001-5053-4543
Xiaoyi Zhang: 0000-0001-9732-1449
Wesley R. Browne: 0000-0001-5063-6961
Jens Uhlig: 0000-0002-0528-0422

### Present Addresses

◆Q.P.: Department of Molecular and Laser Physics, Institute for Molecules and Materials, Radboud University Nijmegen, Heijendaalseweg 135, 6525 AJ Nijmegen, The Netherlands.
¶D.v.D.: Department of Physics at Interfaces, Max Planck Institute for Polymer Research, Ackermannweg 10, D-55128 Mainz, Germany.
+L.F.: Laboratory for Physical Chemistry, ETH Zürich, Vladimir Prelog Weg 1-5/10, 8093 Zürich, Switzerland.
×Q.K.: Science Division, Synchrotron SOLEIL, 91192 Gif-sur-Yvette Cedex, France.

### Author Contributions

◇A.H. and J.U. contributed equally.


### Notes

The authors declare no competing financial interest.

## ACKNOWLEDGMENTS

A.H. acknowledges support by the Dutch Sectorplan for Physics and Chemistry and the Organization for Scientific Research (NWO). Dr. Stefan C. J. Meskers (Technical University of Eindhoven, Eindhoven, The Netherlands) is thanked for his help with the time-resolved photoluminescence experiments. Prof. Johannes G. Vos (Dublin City University, Dublin, Ireland) is acknowledged for scientific discussions. J.U. acknowledges support by the Knut and Alice Wallenberg Stiftelse and the Carl Trygger Stiftelse. Torbjörn Pascher (Pascher Instruments, Lund, Sweden) is acknowledged for his support during the nanosecond TA experiments. G.S. acknowledges the Energy System Integration (ESI) Platform at PSI for funding, support from NCCR MUST. Grant 16.3871.2017/4.6 of the Ministry of Education and Science of the Russian Federation is also acknowledged. This research used resources of the Advanced Photon Source, a U.S. Department of Energy (DOE) Office of Science User Facility operated for the DOE Office of Science by Argonne National Laboratory under Contract DE-AC02-06CH11357. KH and MGL gratefully acknowledge support from DANSCATT for the beamtime activities and MGL further thanks the Danish Council for Independent Research for financial support under Grant DFF-4002-00272.

## REFERENCES


(1) Lewis, N. S.; Nocera, D. G. Powering the Planet: Chemical Challenges in Solar Energy Utilization. *Proc. Natl. Acad. Sci. U. S. A.* **2006**, *103*, 15729−15735.
(2) Sun, L. C.; Hammarstrom, L.; Akermark, B.; Styring, S. Towards Artificial Photosynthesis: Ruthenium−Manganese Chemistry for Energy Production. *Chem. Soc. Rev.* **2001**, *30*, 36−49.
(3) Magnuson, A.; Anderlund, M.; Johansson, O.; Lindblad, P.; Lomoth, R.; Polivka, T.; Ott, S.; Stensjo, K.; Styring, S.; Sundstrom, V.; et al. Biomimetic and Microbial Approaches to Solar Fuel Generation. *Acc. Chem. Res.* **2009**, *42*, 1899−1909.
(4) Hammarstrom, L. Accumulative Charge Separation for Solar Fuels Production: Coupling Light-Induced Single Electron Transfer to Multielectron Catalysis. *Acc. Chem. Res.* **2015**, *48*, 840−850.
(5) Canton, S. E.; Kjaer, K. S.; Vanko, G.; Van Driel, T. B.; Adachi, S. I.; Bordage, A.; Bressler, C.; Chabera, P.; Christensen, M.; Dohn, A. O.; et al. Visualizing the Non-Equilibrium Dynamics of Photoinduced Intramolecular Electron Transfer with Femtosecond X-ray Pulses. *Nat. Commun.* **2015**, *6*, 6359.
(6) Eckenhoff, W. T.; Eisenberg, R. Molecular Systems for Light Driven Hydrogen Production. *Dalton Trans.* **2012**, *41*, 13004−13021.
(7) Losse, S.; Vos, J. G.; Rau, S. Catalytic Hydrogen Production at Cobalt Centres. *Coord. Chem. Rev.* **2010**, *254*, 2492−2504.
(8) Probst, B.; Kolano, C.; Hamm, P.; Alberto, R. An Efficient Homogeneous Intermolecular Rhenium-Based Photocatalytic System for the Production of $H_2$. *Inorg. Chem.* **2009**, *48*, 1836−1843.
(9) Ozawa, H.; Haga, M.; Sakai, K. A Photo-Hydrogen-Evolving Molecular Device Driving Visible-Light-Induced EDTA-Reduction of Water into Molecular Hydrogen. *J. Am. Chem. Soc.* **2006**, *128*, 4926−4927.
(10) Rau, S.; Schafer, B.; Gleich, D.; Anders, E.; Rudolph, M.; Friedrich, M.; Gorls, H.; Henry, W.; Vos, J. G. A Supramolecular Photocatalyst for the Production of Hydrogen and the Selective Hydrogenation of Tolane. *Angew. Chem., Int. Ed.* **2006**, *45*, 6215−6218.
(11) Bressler, C.; Milne, C.; Pham, V. T.; Elnahhas, A.; Van Der Veen, R. M.; Gawelda, W.; Johnson, S.; Beaud, P.; Grolimund, D.; Kaiser, M.; et al. Femtosecond XANES Study of the Light-Induced Spin Crossover Dynamics in an Iron(II) Complex. *Science* **2009**, *323*, 489−492.




DOI: 10.1021/acs.jpca.8b00916
J. Phys. Chem. A 2018, 122, 6396−6406

(12) Smolentsev, G.; Sundstrom, V. Time-Resolved X-ray Absorption Spectroscopy for the Study of Molecular Systems Relevant for Artificial Photosynthesis. *Coord. Chem. Rev.* **2015**, *304-305*, 117−132.
(13) Mara, M. W.; Fransted, K. A.; Chen, L. X. Interplays of Excited State Structures and Dynamics in Copper(I) Diimine Complexes: Implications and Perspectives. *Coord. Chem. Rev.* **2015**, *282-283*, 2−18.
(14) Chábera, P.; Liu, Y.; Prakash, O.; Thyrhaug, E.; El Nahhas, A.; Honarfar, A.; Essén, S.; Fredin, L. A.; Harlang, T. C. B.; Kjær, K. S.; et al. A Low-Spin Fe(III) Complex with 100 ps Ligand-to-Metal Charge Transfer Photoluminescence. *Nature* **2017**, *543*, 695−699.
(15) Hayes, D.; Kohler, L.; Hadt, R. G.; Zhang, X.; Liu, C.; Mulfort, K. L.; Chen, L. X. Excited State Electron and Energy Relays in Supramolecular Dinuclear Complexes Revealed by Ultrafast Optical and X-ray Transient Absorption Spectroscopy. *Chem. Sci.* **2018**, *9*, 860−875.
(16) Van Driel, T. B.; Kjær, K. S.; Hartsock, R. W.; Dohn, A. O.; Harlang, T.; Chollet, M.; Christensen, M.; Gawelda, W.; Henriksen, N. E.; Kim, J. G.; et al. Atomistic Characterization of the Active-Site Solvation Dynamics of a Model Photocatalyst. *Nat. Commun.* **2016**, *7*, 13678.
(17) Ponseca, C. S.; Chábera, P.; Uhlig, J.; Persson, P.; Sundström, V. Ultrafast Electron Dynamics in Solar Energy Conversion. *Chem. Rev.* **2017**, *117*, 10940−11024.
(18) Chen, L. X.; Jäger, W. J. H.; Jennings, G.; Gosztola, D. J.; Munkholm, A.; Hessler, J. P. Capturing a Photoexcited Molecular Structure through Time-Domain X-ray Absorption Fine Structure. *Science* **2001**, *292*, 262−264.
(19) Chen, L. X. Taking Snapshots of Photoexcited Molecules in Disordered Media by Using Pulsed Synchrotron X-rays. *Angew. Chem., Int. Ed.* **2004**, *43*, 2886−2905.
(20) Saes, M.; Bressler, C.; Abela, R.; Grolimund, D.; Johnson, S. L.; Heimann, P. A.; Chergui, M. Observing Photochemical Transients by Ultrafast X-ray Absorption Spectroscopy. *Phys. Rev. Lett.* **2003**, *90*, 047403.
(21) Chergui, M.; Collet, E. Photoinduced Structural Dynamics of Molecular Systems Mapped by Time-Resolved X-ray Methods. *Chem. Rev.* **2017**, *117*, 11025−11065.
(22) Smolentsev, G.; Cecconi, B.; Guda, A.; Chavarot-Kerlidou, M.; Van Bokhoven, J. A.; Nachtegaal, M.; Artero, V. Microsecond X-ray Absorption Spectroscopy Identification of $Co^{I}$ Intermediates in Cobaloxime-Catalyzed Hydrogen Evolution. *Chem. - Eur. J.* **2015**, *21*, 15158−15162.
(23) Moonshiram, D.; Gimbert-Suriñach, C.; Guda, A.; Picon, A.; Lehmann, C. S.; Zhang, X.; Doumy, G.; March, A. M.; Benet-Buchholz, J.; Soldatov, A.; et al. Tracking the Structural and Electronic Configurations of a Cobalt Proton Reduction Catalyst in Water. *J. Am. Chem. Soc.* **2016**, *138*, 10586−10596.
(24) Li, Z.-J.; Zhan, F.; Xiao, H.; Zhang, X.; Kong, Q.-Y.; Fan, X.-B.; Liu, W.-Q.; Huang, M.-Y.; Huang, C.; Gao, Y.-J.; et al. Tracking Co(I) Intermediate in Operando in Photocatalytic Hydrogen Evolution by X-ray Transient Absorption Spectroscopy and DFT Calculation. *J. Phys. Chem. Lett.* **2016**, *7*, 5253−5258.
(25) Kowacs, T.; O'Reilly, L.; Pan, Q.; Huijser, A.; Lang, P.; Rau, S.; Browne, W. R.; Pryce, M. T.; Vos, J. G. Subtle Changes to Peripheral Ligands Enable High Turnover Numbers for Photocatalytic Hydrogen Generation with Supramolecular Photocatalysts. *Inorg. Chem.* **2016**, *55*, 2685−2690.
(26) Pan, Q.; Mecozzi, F.; Korterik, J. P.; Vos, J. G.; Browne, W. R.; Huijser, A. The Critical Role Played by the Catalytic Moiety in the Early-Time Photodynamics of Hydrogen Generating Bimetallic Photocatalysts. *ChemPhysChem* **2016**, *17*, 2654−2659.
(27) Tschierlei, S.; Karnahl, M.; Presselt, M.; Dietzek, B.; Guthmuller, J.; Gonzalez, L.; Schmitt, M.; Rau, S.; Popp, J. Photochemical Fate: The First Step Determines Efficiency of $H_2$ Formation with a Supramolecular Photocatalyst. *Angew. Chem., Int. Ed.* **2010**, *49*, 3981−3984.
(28) Pan, Q.; Freitag, L.; Kowacs, T.; Falgenhauer, J. C.; Korterik, J. P.; Schlettwein, D.; Browne, W. R.; Pryce, M. T.; Rau, S.; Gonzalez, L.; et al. Peripheral Ligands as Electron Storage Reservoirs and Their Role in Enhancement of Photocatalytic Hydrogen Generation. *Chem. Commun.* **2016**, *52*, 9371−9374.
(29) Pan, Q.; Mecozzi, F.; Korterik, J. P.; Sharma, D.; Herek, J. L.; Vos, J. G.; Browne, W. R.; Huijser, A. Directionality of Ultrafast Electron Transfer in a Hydrogen Evolving Ru−Pd-Based Photocatalyst. *J. Phys. Chem. C* **2014**, *118*, 20799−20806.
(30) Bhasikuttan, A. C.; Okada, T. Excited-State Relaxation Dynamics of $Ru(dcbpy)_2(NCS)_2$, Studied by Fluorescence Upconversion Spectroscopy. *J. Phys. Chem. B* **2004**, *108*, 12629−12632.
(31) Hartley, F. R. *The Chemistry of Platinum and Palladium: With Particular Reference to Complexes of the Elements*; Applied Science Publishers: London, 1973.
(32) Williams, J. A. G. Photochemistry and Photophysics of Coordination Compounds: Platinum. *Top. Curr. Chem.* **2007**, *281*, 205−268.
(33) Singh Bindra, G.; Schulz, M.; Paul, A.; Groarke, R.; Soman, S.; Inglis, J. L.; Browne, W. R.; Pfeffer, M. G.; Rau, S.; Maclean, B. J.; et al. The Role of Bridging Ligand in Hydrogen Generation by Photocatalytic Ru/Pd Assemblies. *Dalton Trans.* **2012**, *41*, 13050−13059.
(34) Ha, K. Crystal Structure of (Acetonitrile-κN)chlorido[2-(2-pyridyl)phenyl-$\kappa^2$N,C]platinum(II), $C_{13}H_{11}ClN_2Pt$. *Z. Kristallogr. - New Cryst. Struct.* **2014**, *229*, 151−152.
(35) Miller, J. S.; Min, K. S. Oxidation Leading to Reduction: Redox-Induced Electron Transfer (RIET). *Angew. Chem., Int. Ed.* **2009**, *48*, 262−272.
(36) Nabavizadeh, S. M.; Amini, H.; Rashidi, M.; Pellarin, K. R.; Mccready, M. S.; Cooper, B. F. T.; Puddephatt, R. J. The Mechanism of Oxidative Addition of Iodine to a Dimethylplatinum(II) Complex. *J. Organomet. Chem.* **2012**, *713*, 60−67.
(37) Canton, S. E.; Zhang, X. Y.; Zhang, J. X.; Van Driel, T. B.; Kjaer, K. S.; Haldrup, K.; Chabera, P.; Harlang, T.; Suarez-Alcantara, K.; Liu, Y. Z.; et al. Toward Highlighting the Ultrafast Electron Transfer Dynamics at the Optically Dark Sites of Photocatalysts. *J. Phys. Chem. Lett.* **2013**, *4*, 1972−1976.
(38) Snellenburg, J. J.; Laptenok, S. P.; Seger, R.; Mullen, K. M.; Van Stokkum, I. H. M. Glotaran: A Java-Based Graphical User Interface for the R Package TIMP. *J. Stat. Softw.* **2012**, *49*, 1−22.
(39) Jones, E.; Oliphant, T.; Peterson, P.; et al. SciPy: Open-Source Scientific Tools for Python. http://www.scipy.org/ (accessed Dec 15, 2017).
(40) Oang, K. Y.; Yang, C.; Muniyappan, S.; Kim, J.; Ihee, H. SVD-Aided Pseudo Principal-Component Analysis: A New Method To Speed Up and Improve Determination of the Optimum Kinetic Model from Time-Resolved Data. *Struct. Dyn.* **2017**, *4*, 044013.
(41) Ruckebusch, C.; Sliwa, M.; Pernot, P.; De Juan, A.; Tauler, R. Comprehensive Data Analysis of Femtosecond Transient Absorption Spectra: A Review. *J. Photochem. Photobiol., C* **2012**, *13*, 1−27.
(42) Van Stokkum, I. H. M.; Larsen, D. S.; Van Grondelle, R. Global and Target Analysis of Time-Resolved Spectra. *Biochim. Biophys. Acta, Bioenerg.* **2004**, *1657*, 82−104.
(43) Ravel, B.; Newville, M. Athena, Artemis, Hephaestus: Data Analysis for X-ray Absorption Spectroscopy Using Ifeffit. *J. Synchrotron Radiat.* **2005**, *12*, 537−541.
(44) Bunker, G. *Introduction to XAFS: A Practical Guide to X-ray Absorption Fine Structure Spectroscopy*; Cambridge University Press: Cambridge, U.K., 2010.
(45) Calvin, S. *XAFS for Everyone*; CRC Press: Boca Raton, FL, 2013.
(46) Rehr, J. J.; Kas, J. J.; Vila, F. D.; Prange, M. P.; Jorissen, K. Parameter-Free Calculations of X-ray Spectra with FEFF9. *Phys. Chem. Chem. Phys.* **2010**, *12*, 5503−5513.
(47) Smolentsev, G.; Soldatov, A. V. FitIt: New Software To Extract Structural Information on the Basis of XANES Fitting. *Comput. Mater. Sci.* **2007**, *39*, 569−574.


DOI: 10.1021/acs.jpca.8b00916
J. Phys. Chem. A 2018, 122, 6396−6406

(48) Seabold, S.; Perktold, J. Statsmodels: Econometric and Statistical Modeling with Python. In *Proceedings of the 9th Python in Science Conference*, 2010.
(49) Kobayashi, M.; Masaoka, S.; Sakai, K. Syntheses, Characterization, and Photo-Hydrogen-Evolving Properties of Tris(2,2′-bipyridine)ruthenium(II) Derivatives Tethered to an $H_2$-Evolving (2-Phenylpyridinato)platinum(II) Unit. *Molecules* **2010**, *15*, 4908−4923.
(50) Damrauer, N. H.; Cerullo, G.; Yeh, A.; Boussie, T. R.; Shank, C. V.; McCusker, J. K. Femtosecond Dynamics of Excited-State Evolution in $[Ru(bpy)_3]^{2+}$. *Science* **1997**, *275*, 54−57.
(51) Cannizzo, A.; Van Mourik, F.; Gawelda, W.; Zgrablic, G.; Bressler, C.; Chergui, M. Broadband Femtosecond Fluorescence Spectroscopy of $[Ru(bpy)_3]^{2+}$. *Angew. Chem., Int. Ed.* **2006**, *45*, 3174−3176.
(52) Atkins, A. J.; González, L. Trajectory Surface-Hopping Dynamics Including Intersystem Crossing in $[Ru(bpy)_3]^{2+}$. *J. Phys. Chem. Lett.* **2017**, *8*, 3840−3845.
(53) Battocchio, C.; D'acapito, F.; Smolentsev, G.; Soldatov, A. V.; Fratoddi, I.; Contini, G.; Davoli, I.; Polzonetti, G.; Mobilio, S. XAS Study of a Pt-Containing Rod-Like Organometallic Polymer. *Chem. Phys.* **2006**, *325*, 422−428.
(54) Lockard, J. V.; Rachford, A. A.; Smolentsev, G.; Stickrath, A. B.; Wang, X. H.; Zhang, X. Y.; Atenkoffer, K.; Jennings, G.; Soldatov, A.; Rheingold, A. L.; et al. Triplet Excited State Distortions in a Pyrazolate Bridged Platinum Dimer Measured by X-ray Transient Absorption Spectroscopy. *J. Phys. Chem. A* **2010**, *114*, 12780−12787.
(55) Tsai, Y. W.; Tseng, Y. L.; Sarma, L. S.; Liu, D. G.; Lee, J. F.; Hwang, B. J. Genesis of Pt Clusters in Reverse Micelles Investigated by in Situ X-ray Absorption Spectroscopy. *J. Phys. Chem. B* **2004**, *108*, 8148−8152.
(56) Hall, M. D.; Foran, G. J.; Zhang, M.; Beale, P. J.; Hambley, T. W. Xanes Determination of the Platinum Oxidation State Distribution in Cancer Cells Treated with Platinum(IV) Anticancer Agents. *J. Am. Chem. Soc.* **2003**, *125*, 7524−7525.
(57) Yahav, A.; Goldberg, I.; Vigalok, A. Iodine Oxidative Addition to Isomeric Platinum(II) Phosphine Complexes. *Organometallics* **2005**, *24*, 5654−5659.
(58) Van Beek, J. A.; Van Koten, G.; Smeets, W. J.; Spek, A. L. Model for the Initial Stage in the Oxidative Addition of $I_2$ to Organoplatinum(II) Compounds. X-ray Structure of Square-Pyramidal $[Pt^{II}I\{C_6H_3(CH_2NMe_2)_2\text{-}o,o'\}(\eta^1\text{-}I_2)]$ Containing a Linear Pt−I−I Arrangement. *J. Am. Chem. Soc.* **1986**, *108*, 5010−5011.
(59) Gossage, R. A.; Ryabov, A. D.; Spek, A. L.; Stufkens, D. J.; Van Beek, J. A.; Van Eldik, R.; Van Koten, G. Models for the Initial Stages of Oxidative Addition. Synthesis, Characterization, and Mechanistic Investigation of $\eta^1$-$I_2$ Organometallic "Pincer" Complexes of Platinum. X-ray Crystal Structures of $[PtI(C_6H_3\{CH_2NMe_2\}_2\text{-}2,6)(\eta^1\text{-}I_2)]$ and *exo-meso*-$[Pt(\eta^1\text{-}I_3)(\eta^1\text{-}I_2)(C_6H_3\{CH_2N(t\text{-}Bu)Me\}_2\text{-}2,6)]$. *J. Am. Chem. Soc.* **1999**, *121*, 2488−2497.
(60) Suneesh, C. V.; Balan, B.; Ozawa, H.; Nakamura, Y.; Katayama, T.; Muramatsu, M.; Nagasawa, Y.; Miyasaka, H.; Sakai, K. Mechanistic Studies of Photoinduced Intramolecular and Intermolecular Electron Transfer Processes in RuPt-Centred Photo-Hydrogen-Evolving Molecular Devices. *Phys. Chem. Chem. Phys.* **2014**, *16*, 1607−1616.
(61) Kobayashi, M.; Masaoka, S.; Sakai, K. Synthesis, Crystal Structure, Solution and Spectroscopic Properties, and Hydrogen-Evolving Activity of [K(18-Crown-6)][Pt(II)(2-Phenylpyridinato)-$Cl_2$]. *Photochem. Photobiol. Sci.* **2009**, *8*, 196−203.
(62) Kowacs, T.; Pan, Q.; Lang, P.; O'reilly, L.; Rau, S.; Browne, W. R.; Pryce, M. T.; Huijser, A.; Vos, J. G. Supramolecular Bimetallic Assemblies for Photocatalytic Hydrogen Generation from Water. *Faraday Discuss.* **2015**, *185*, 143−170.
(63) Hammarström, L. Accumulative Charge Separation for Solar Fuels Production: Coupling Light-Induced Single Electron Transfer to Multielectron Catalysis. *Acc. Chem. Res.* **2015**, *48*, 840−850.
(64) Pfeffer, M. G.; Schäfer, B.; Smolentsev, G.; Uhlig, J.; Nazarenko, E.; Guthmuller, J.; Kuhnt, C.; Wächtler, M.; Dietzek, B.; Sundström, V.; et al. Palladium Versus Platinum: The Metal in the Catalytic Center of a Molecular Photocatalyst Determines the Mechanism of the Hydrogen Production with Visible Light. *Angew. Chem., Int. Ed.* **2015**, *54*, 5044−5044.
(65) Pfeffer, M. G.; Kowacs, T.; Wächtler, M.; Guthmuller, J.; Dietzek, B.; Vos, J. G.; Rau, S. Optimization of Hydrogen-Evolving Photochemical Molecular Devices. *Angew. Chem., Int. Ed.* **2015**, *54*, 6627−6631.


DOI: 10.1021/acs.jpca.8b00916
*J. Phys. Chem. A* 2018, 122, 6396−6406